2016 IEEE 66th Electronic Components and Technology Conference

A Novel Approach to Integrating 3D/4D Printing and Stretchable Conductive adhesive Technologies for High Frequency Packaging Applications

Taoran Le[1], Chia-Chi Tuan[2], Ryan A. Bahr[1], C. P. Wong[2], and M. M. Tentzeris[1]
[1]School of ECE, [2]School of Materials Science and Engineering,
Georgia Institute of Technology
Atlanta, GA 30332
taoran.le@ece.gatech.edu

***Abstract*—This paper demonstrates a new method for the free standing 3D printing of a polyurethane (PU)-based electrically conductive adhesive (ECA). Due to the special mechanical and electrical properties of the in-house-made ECAs [1, 2], which has an ultralow resistivity of ≈1.0 × 10^{-5} Ωcm, our approach opens new avenues for creating soft electronics applications, such as strain sensors [3], soft robotics [4, 5] and flexible, wearable RF devices [6]. A proof-of-concept fractal 3D Hilbert dipole antenna at 433 MHz ISM band is designed and fabricated by this method.**

Keyword—3D printing; materiel characterization; 3D Hilbert antenna; ECA; flexible electronics; RF.

I. INTRODUCTION

Historically, the primary focus of electronic devices has been on rigid devices. In the last decade wearable electronics [6, 7], soft robotics [4, 5] and flexible displays [8], etc., have been striving for a new class of electronic devices - flexible/stretchable electronics. However, flexible/stretchable electronics impose a stringent requirement for interconnect materials [9, 10]. In addition to the conventional functions of providing sufficient power, ground, and signal transmission, interconnects for flexible electronics are required to maintain excellent mechanical robustness and electrical interconnectivity during mechanical deformation [1].

Surface mount technology (SMT) and flip-chip interconnection on flexible and low-cost substrate in flexible electronics require electrically conductive adhesive (ECA) with high electrical conductivity, low process temperature, good mechanical compliance, and strong adhesion [1]. A commonly used approach is to maintain the conventional circuit layout but embed stretchable or flowable conductive materials, such as conductive polymers [11] conductive polymer composites [12], and liquid metal alloys [13] as stretchable conductive lines. In this paper we chose to use flexible ECAs as the conductive material. The ECAs feature a higher conductivity (8.4×10^6 Sm^{-1}) than most previously reported flexible/stretchable conductors [12, 14]. More importantly, the conductivity of our ECAs is as high as 1.11×10^5 Sm^{-1} at a strain of 240% and remains almost invariant over 500 cycles of stretching at 100% applied strain [2]. These ECAs are highly suitable for building flexible/stretchable RF devices.

To create the desired design geometries of flexible electronics, a number of processing methods have been employed to date, including lithographic [15, 16], stencil printing [1, 6], coating and micro-channel molding, filling techniques[17, 18]. However, these methods are high-cost, lack manufacturing scalability, or employ complicated processes, which have limited their widespread adoption. In contrast, 3D printing does not suffer these limitations and has already started becoming one of the mainstream additive printing technologies and works by building physical objects up layer by layer, based on detailed digital blueprints [19]. The advantages of 3D printing technology include time savings and the capability to fabricate complex structures with multiple materials, which is beyond the capability of traditional fabrication methods.

The rapid growth in 3D and 4D (time-reconfigurable) printing technology offers unique advantages in terms of optimal non-orthogonal shapes, on-demand deposition of nanostructures and antennas, as well as multilayer stretchable hermetic RF packages for flexible RF modules. However, there are significant barriers to the fabrication of fully 3D multilayer structures. One of these barriers is the overhang or bridge problem, where the structures are affected by gravity during the printing process. Most designs therefore try to avoid extreme overhang 3D structures and favor printing electrical circuits on a surface, such as in [3, 20]. Strictly speaking, these techniques belong to the 2.5D printing category. The current market offers three solutions for printing extreme overhang structures: zero support, rigid support structure and non-rigid support material. Zero support is still in the early stages [21] and still there exist many limitations in the selection of printing material and geometry design. Rigid support structures are the most common solution for extreme overhang designs. However, it wastes material, is time consuming, and it is hard to remove the support, which usually leaves small marks on the printed object, causing dimensional inaccuracies. For non-rigid support materials, powder based technologies, like selective laser sintering (SLS) and direct metal laser Sintering (DMLS), are widely used printing methods in the market. They can use the surrounding powder itself to hold everything in place, such as 3DPandoras printer [22]. However, the powder can be difficult to remove, especially when printing metal or nylon. Other early stage methods, such as embedded 3D printing [23], are still not mature enough as the utilized ink. The ink requires high resistivity (117 Ω·cm) and the printing process is complicated.

In this paper, we are planning to present a fully 3D printed stretchable/flexible on-package antenna by ECA in a support bath. This method involves extruding in-house-made ECA through a deposition needle directly into a polydimethylsiloxane (PDMS) resin bath. The gel bath serves as a support material for full 3D printing. As the needle transports in the bath it introduces a void space, which is filled

978-1-5090-1204-6/16 $31.00 © 2016 IEEE
DOI 10.1109/ECTC.2016.346

by ECA at the same time. This viscoelastic ECA can be extruded through the fine deposition needle. Due to the surface tension difference between PDMS and ECA, no mixing occurs between the ECA and the PDMS bath. After printing, the printed object is cured at 150 °C, while the PDMA bath remains fluid. The whole printing process is highly programmable. A fractal 3D Hilbert dipole antenna was designed in the commercial full wave simulator in CST MICROWAVE STUDIO® as a preliminary proof-of-concept prototype. The antenna is made of in-house-made ECA. The printing process is illustrated in the Fig.1.

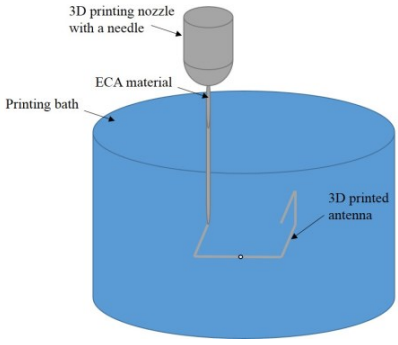

Fig.1. A fractal 3D Hilbert dipole antenna under 3D printing process in the support bath.

The material preparation and the detailed 3D printing process are presented in Section II. The 3D Hilbert antenna design and printed process are discussed in Section III and IV, respectively. Lastly, Section V presents the future work of the characterization of this 3D Hilbert dipole antenna.

II. 3D PRINTING PREPARATION AND ECA FORMULATION

There are several criteria for properly printing ECA in a supporting bath. First, the ECA must immediately fill the void space created during the needle's movement. Second, the ECA and the bath must be chemically compatible during the printing and curing process as well as exhibit appropriate mechanical and electrical properties. Third, after printing, the gel bath must facilitate patterning the designed 3D structure without breakup. Fourth, the gel bath must flow into the void space quickly enough after the needle passes where it does not deposit ECA. Lastly, after the curing, the gel bath should remain fluid to enable its easy removal.

To meet these requirements, we designed a novel approach to develop a novel polyurethane (PU)-based flexible ECA (PU-ECA) and a PDMS resin as the gel bath.

A. ECA formulation and fabrication

Elastomers that provide better adhesion strengths, such as PU, has been thoroughly investigated. In addition to the improved adhesion strength, the isocyanate groups in the PU matrix are relatively reactive and thus provide increased versatility for matrix modification. The PU resin used is a hexamethylene diisocyanate (HDI) and is cured by polyethylene glycol (PEG, Mw=400). Dibutyltin dilaurate is used as the curing catalyst. Two silver flakes with different sizes from Ames Advanced Materials Corporation were used to improve the packing density and adjust the viscosity of the formulated pastes. HDI and PEG were degassed in a vacuum oven overnight before mixing with 80 wt.% silver flakes and each of the two grades of silver was added by the same amount. The mixture was homogenized to form the ECA paste. The pastes were thermally cured at 150°C for 1 hour.

The PEG 400, selected as an optimized chain length of PEG, was based on three aspects: the low bulk resistivity of the PU-ECA, low Young's modulus, and low glass-transition temperature (T_g) of the PU cured with PEG. The bulk resistivity of PU-ECA prepared with PEG of different lengths is shown in Fig.2.. The resistivity increases with PEG chain length at the same filler loading. The Young's moduli decrease with the increase of PEG molecular weight, shown in Fig. 3.. The DSC results of cured PU with different PEG chain lengths are demonstrated in Fig.4.. PEG with molecular weights of 200 g mol-1 (PEG 200) and 400g g mol-1 (PEG 400) does not form crystallites while PEG 400 has a lower T_g (-25 °C) than that PEG 200 (6 °C) The lower T_g renders consistent mechanical properties in a larger temperature window.

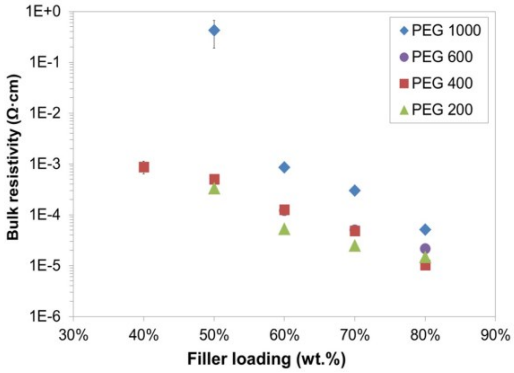

Fig.2. Bulk resistivity of PU ECAs as a function of silver loading for PU resin prepared with different molecular weight PEG

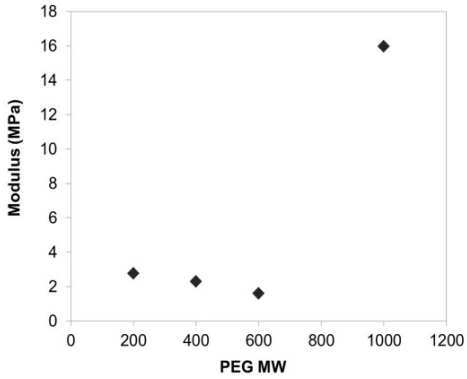

Fig.3. Young's modulus of PU resin prepared with different molecular weight PEG

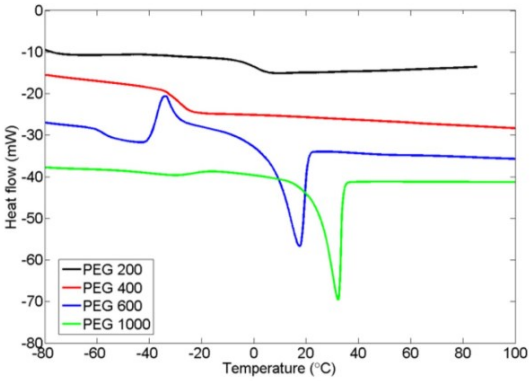

Fig.4. DSC results of PU resin prepared with different molecular weight PEG

The electrical conductivity can be improved in two ways: the significant shrinkage of PU-ECA during the curing process leads to an increased volume percentage of silver. The second possible factor is the fact that the hydroxyl groups in the polyether chains can reduce the silver salts on the surface of silver flakes in situ to produce silver nanoparticles, which can be sintered during curing to form metallic bridges between neighboring flakes [1].

B. ECA material characterization

Low resistivity is one of the most critical requirements for the ECAs to be used in stretchable RF devices, like antennas, because it will affect the conduction loss and thus the radiation efficiency. To measure the electrical resistivity, two strips of Kapton® tape were applied onto a glass slide. The formulated paste was printed on the glass slide. After curing, the bulk resistance of ECA strips was measured following the typical four-probe method with a Keithley 2000 multimeter. The width and length were measured by a caliper and the thickness was measured by a profile meter (Heidenhain ND 281, Germany). The bulk resistivity ρ was then calculated by

$$\rho = \frac{wt}{l} \tag{1}$$

where l, w, and t are the length, width and thickness of the strip, respectively. The bulk resistivity is around 1.19×10^{-5} **Ω**·cm at 80 wt.% silver loading when cured at 150°C, which is comparable with conventional epoxy-based ECAs and in the same order of magnitude with many metals.

The viscosity of ECA was measured using a DHR-2 rheometer (TA Instruments). A parallel-plate geometry with 25 mm plates was used, and measurements were made for shear rates of 0.1 Hz to 100 Hz and are shown in Fig. 5.. The viscosity of ECA at 0.1 Hz is around 335 Pa*s.

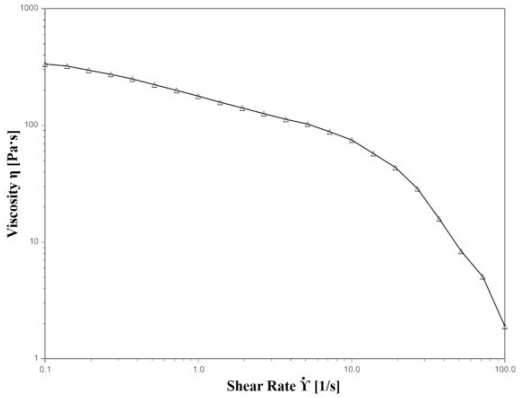

Fig. 5. The apparent viscosity of ECA as a function of shear rate

C. 3D printing ECA

Most commercial low-cost 3D printers today use fused deposition modeling (FDM). This technology feeds printing material into an extruder and then precisely lays down the material. A variety of adjustable options of this technique affect the printing quality. The most of important properties include layer height, amount of top and bottom solid layers, amount of perimeter walls, solid/infill patterns, and infill densities.

The 3D antenna prototype presented in this paper was fabricated by a 100% infill density ECA. All samples tested are made on the Hyrel System 30 3D printer [24], as shown in Fig. 6 (a). This hardware uses a modified version of the Repetier controller software called Repetrel, which still uses the common slicing CAD software slic3r [25, 26]. The Hyrel EMO-25 extruder was loaded a 6ml ECA syringe with a 27 gauge needle, as presented in Fig.6 (b).

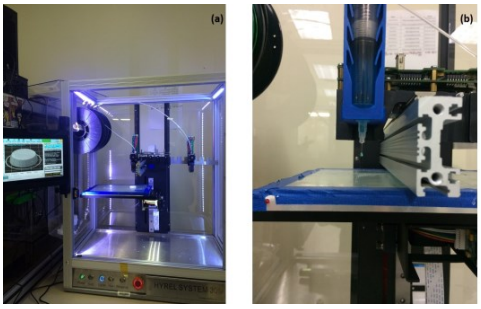

Fig. 6. (a) Hyrel System 30 3D printer; (b) EMO-25 extruder is ready to print ECA (S-video1).

D. PDMS support bath

PDMS resin was degassed in a vacuum oven overnight, then dispensed into a glass bottle inside which the ECA was to be printed. Due to the surface tension difference between PDMS, HDI, and PEG, no mixing occurs between the ECA and the PDMS bath. Negligible viscosity and density variation is observed in PDMS over a wide temperature range, allowing the 3D-printed ECA structure to be preserved throughout the printing and curing process. Different viscosity PDMS baths were made by using PDMS of different molecular weights for use in trials of printing ECA. As shown in Fig.7, the PDMS bath that best retains the original printed shape and position

after curing, was chosen. Fig.7 (b) shows how the failed ECA shape on the right sank to the bottom of the bottle. After curing the ECA, the PDMS bath was removed to yield the final 3D antenna.

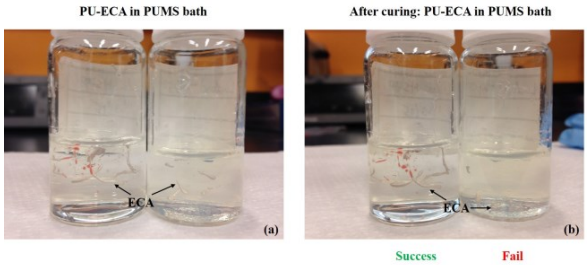

Fig. 7. The comparison of Success vs. Fail of 3D printing ECA in the PDMS bath.

The viscosity of the successful PDMS bath was measured using the DHR-2 rheometer. A parallel-plate geometry with 25 mm plates was used, and the measurements was made for shear rates of 0.1 Hz to 100 Hz and are shown in Fig. 8.. The viscosity of the successful PDMS bath is approximately 623 Pa*s.

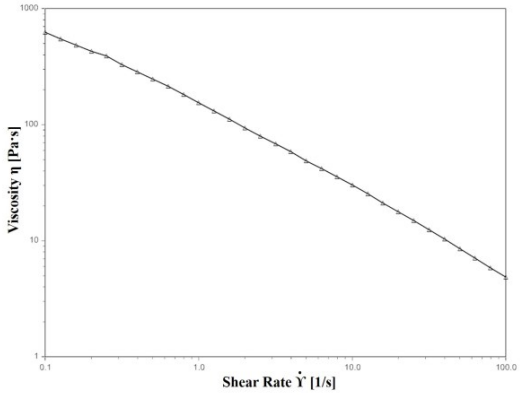

Fig. 8. The apparent viscosity of PDMS bath as a function of shear rate

III. 3-DIMENSIONAL HILBERT ANTENNA

A. 3D Hilbert antenna

To demonstrate the applicability of 3D printed ECA to RF devices, a first iteration of a fractal 3D Hilbert dipole antenna was designed. Fractal refers to the complex geometries that are created through successive iterations when applying a geometric generator to a simple Euclidean basis or iteration geometry [27]. In short, a small region of the geometry repeats the whole geometry in a space-filling way [28]. These space-filling type of curves had been extensively utilized for designing multiband and miniaturized antennas [29-31], which are important for RF packaging applications. One of the most widely used fractal curves is the 3D Hilbert curve, which was proposed by Hilbert in 1891. Hilbert antennas exhibit better Q factor than the equivalent loaded dipole antennas. This includes another fractal antenna, the Koch antenna [27]. The first three iterations of a fractal 3D Hilbert dipole antenna geometry are shown in Fig.9.. To prove our 3D printing concept, we chose to use the first iteration of a fractal 3D Hilbert dipole antenna.

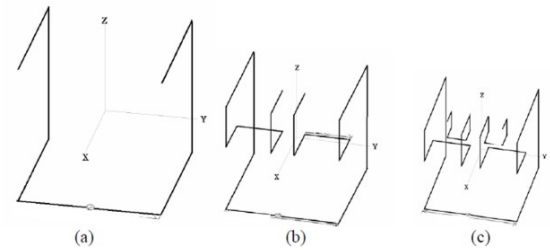

Fig. 9. The first three iterations of the 3D-fractal Hilbert dipole antennas

Wireless wearable communication is a field of increasing research in flexible electronics, especially for on-body body sensor network (BSN) applications. The 433 MHz ISM band is used mostly by implanted sensors and thus allows for their easier integration into a BSN [32], thus it was chosen for the first iteration of the 3D printed fractal 3D Hilbert dipole antenna prototype. A first iteration of fractal 3D Hilbert dipole antenna at 433 MHz band has been designed.

B. Simulation results

The geometry of the proposed dipole antenna is depicted in Fig. 10.. The dipole antenna is made of PU-ECAs. The wire radius of the antenna is 0.1 cm. The feed port of the dipole is right in the center connected with a 73 Ω source. The two arms extend to form the first iteration of 3D Hilbert curve. The ECA's conductivity is 8.4×10^{6} Sm^{-1} in the simulation. The simulated S_{11} parameter of the antenna is shown in Fig. 11..

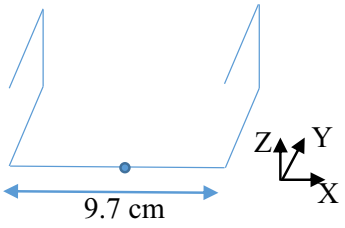

Fig.10. The geometry of the 3D Hilbert dipole antenna

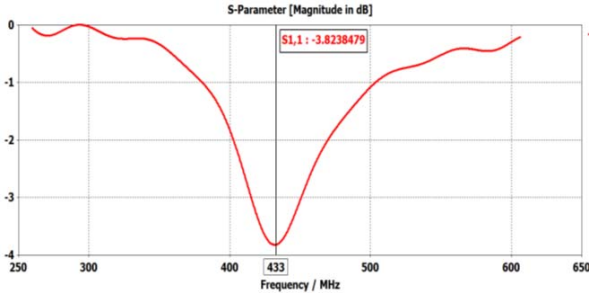

Fig.11. S_{11} of the 3D Hilbert dipole antenna

IV. 3D PRINTED 3 DIMENSIONAL HILBERT ANTENNA

During 3D printing, the needle has to always move up to avoid damaging the already printed object. As shown in Fig.12., three steps are involved to print this fractal 3D Hilbert antenna. The first step is for the bottom, labeled (1) and marked in a purple color. The second step is to print the left arm, labeled (2) and shown in red. The third step is to print the right arm, labeled (3) and shown in yellow. After curing, the antenna keeps the original shape and position in the PDMS bath as expected.

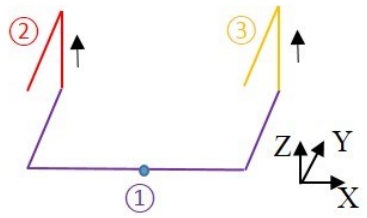

Fig.12. 3D printing steps for the fractal 3D Hilbert antenna

V. FUTURE WORK

A properly chosen off-center feed point of 3D Hilbert antenna may provide an approximate 73 Ω real input impedance at the fundamental resonant frequency of this antenna. The impedance-matching circuits can be another solution, but it may complicate the design. We plan to reprint the 3D Hilbert antenna in a bottle with a hole at the bottle. So the coaxial cable can go through it to connect between the printed antenna and a R&S® ZVA8 vector network analyzer (VNA). The resolution of the PU-ECA can be improved by modifying the printing needle size.

VI. CONCLUSIONS

We report a new method for fully 3D printing flexible ECA in PDMS support bath. We create a low cost PU-ECA with decent flexibility and extra-high conductivity for flexible electronics. And it can be printed smoothly on a commercial 3D printer – Hyrel 3D printer with around 200 um resolutions. We also found a proper viscosity of support bath for this PU-ECA during fully 3D printing work. A fractal 3D Hilbert dipole antenna was successfully fully 3D printed by utilizing this method. Our approach opens new avenues for creating soft electronics for wearable RF circuits, soft robotics, 3D flexible sensors, and beyond.

ACKNOWLEDGMENTS

The authors would like to thank DTRA and NSF-EFRI for their support of the research. The authors are also grateful for the useful discussion with Dr. Joshua C. Agar at University of California Berkeley.

REFERENCES

[1] Z. Li, R. Zhang, K. S. Moon, Y. Liu, K. Hansen, T. Le, *et al.*, "Highly Conductive, Flexible, Polyurethane Based Adhesives for Flexible and Printed Electronics," *Advanced Functional Materials,* vol. 23, pp. 1459-1465, 2013.

[2] Z. Li, T. Le, Z. Wu, Y. Yao, L. Li, M. Tentzeris, *et al.*, "Rational Design of a Printable, Highly Conductive Silicone based Electrically Conductive Adhesive for Stretchable Radio Frequency Antennas," *Advanced Functional Materials,* vol. 25, pp. 464-470, 2015.

[3] T. Le, B. Song, Q. Liu, R. A. Bahr, S. Moscato, C.-P. Wong, *et al.*, "A novel strain sensor based on 3D printing technology and 3D antenna design," in *Electronic Components and Technology Conference (ECTC), 2015 IEEE 65th*, 2015, pp. 981-986.

[4] A. Levi, M. Piovanelli, S. Furlan, B. Mazzolai, and L. Beccai, "Soft, transparent, electronic skin for distributed and multiple pressure sensing," *Sensors,* vol. 13, pp. 6578-6604, 2013.

[5] R. V. Martinez, J. L. Branch, C. R. Fish, L. Jin, R. F. Shepherd, R. Nunes, *et al.*, "Robotic tentacles with three dimensional mobility based on flexible elastomers," *Advanced Materials,* vol. 25, pp. 205-212, 2013.

[6] T. Le, R. A. Bahr, M. M. Tentzeris, B. Song, and C.-p. Wong, "A novel chipless RFID-based stretchable and wearable hand gesture sensor," in *Microwave Conference (EuMC), 2015 European*, 2015, pp. 371-374.

[7] S. Xu, Y. Zhang, L. Jia, K. E. Mathewson, K.-I. Jang, J. Kim, *et al.*, "Soft microfluidic assemblies of sensors, circuits, and radios for the skin," *Science,* vol. 344, pp. 70-74, 2014.

[8] S.-I. Park, Y. Xiong, R.-H. Kim, P. Elvikis, M. Meitl, D.-H. Kim, *et al.*, "Printed assemblies of inorganic light-emitting diodes for deformable and semitransparent displays," *science,* vol. 325, pp. 977-981, 2009.

[9] B. D. Gates, "Flexible electronics," *Science,* vol. 323, pp. 1566-1567, 2009.

[10] J. A. Rogers, T. Someya, and Y. Huang, "Materials and mechanics for stretchable electronics," *Science,* vol. 327, pp. 1603-1607, 2010.

[11] A. Verma, B. Weng, R. Shepherd, C. Fumeaux, V.-T. Truong, G. G. Wallace, *et al.*, "6 GHz microstrip patch antennas with PEDOT and polypyrrole conducting polymers," in *Electromagnetics in Advanced Applications (ICEAA), 2010 International Conference on*, 2010, pp. 329-332.

[12] J. Agar, J. Durden, D. Staiculescu, R. Zhang, E. Gebara, and C. Wong, "Electrically conductive silicone nano-composites for stretchable RF devices," in *Microwave Symposium Digest (MTT), 2011 IEEE MTT-S International*, 2011, pp. 1-4.

[13] M. Kubo, X. Li, C. Kim, M. Hashimoto, B. J. Wiley, D. Ham, *et al.*, "Stretchable microfluidic radiofrequency antennas," *Advanced Materials,* vol. 22, pp. 2749-2752, 2010.

[14] Z. Li, K. Hansen, Y. Yao, Y. Ma, K.-s. Moon, and C. Wong, "The conduction development mechanism of silicone-based electrically conductive adhesives," *Journal of Materials Chemistry C,* vol. 1, pp. 4368-4374, 2013.

[15] D. H. Kim, Y. S. Kim, J. Wu, Z. Liu, J. Song, H. S. Kim, *et al.*, "Ultrathin silicon circuits with strain isolation layers and mesh layouts for high performance electronics on fabric, vinyl, leather, and paper," *Advanced Materials,* vol. 21, pp. 3703-3707, 2009.

[16] H. C. Ko, M. P. Stoykovich, J. Song, V. Malyarchuk, W. M. Choi, C.-J. Yu, *et al.*, "A hemispherical electronic eye camera based on compressible silicon optoelectronics," *Nature,* vol. 454, pp. 748-753, 2008.

[17] J.-B. Chossat, Y.-L. Park, R. J. Wood, and V. Duchaine, "A soft strain sensor based on ionic and metal liquids," *Sensors Journal, IEEE,* vol. 13, pp. 3405-3414, 2013.

[18] D. M. Vogt, Y.-L. Park, and R. J. Wood, "Design and characterization of a soft multi-axis force sensor using embedded microfluidic channels," *Sensors Journal, IEEE,* vol. 13, pp. 4056-4064, 2013.

[19] M. Frauenfelder, *Make: Ultimate guide to 3D printing 2014*: Maker Media, Inc., 2013.

[20] J. J. Adams, E. B. Duoss, T. F. Malkowski, M. J. Motala, B. Y. Ahn, R. G. Nuzzo, *et al.*, "Conformal Printing of Electrically Small Antennas on Three Dimensional Surfaces," *Advanced Materials,* vol. 23, pp. 1335-1340, 2011.

[21] C. Ladd, J. H. So, J. Muth, and M. D. Dickey, "3D printing of free standing liquid metal microstructures," *Advanced Materials,* vol. 25, pp. 5081-5085, 2013.

[22] (2016). *3DPandoras: The first full color 3d printer of powder tech.* Available: http://3dpandoras.com/

[23] J. T. Muth, D. M. Vogt, R. L. Truby, Y. i. Meng, D. B. Kolesky, R. J. Wood, *et al.*, "Embedded 3D printing of strain sensors within highly stretchable elastomers," *Advanced Materials,* vol. 26, pp. 6307-6312, 2014.

[24] (2016). *Hyrel 3D*. Available: http://www.hyrel3d.com/

[25] (2015). *Recreus 3D printing materials. Elastic & flexible filament Filaflex - Recreus.com*. Available: http://recreus.com/en/

[26] (2016). - *Repetier Software*. Available: http://www.repetier.com/

[27] H. Elkamchouchi and M. A. Nasr, "3D-fractal rectangular Koch Dipole and Hilbert Dipole antennas," in *Microwave and Millimeter Wave Technology, 2007. ICMMT'07. International Conference on*, 2007, pp. 1-4.

[28] B. Mandelbrot Benoit, "The fractal geometry of nature," *Henry Holt and Company,* 1983.

[29] K. Vinoy, K. Jose, V. Varadan, and V. Varadan, "Hilbert curve fractal antenna: A small resonant antenna for VHF/UHF applications," *Microwave and Optical Technology Letters,* vol. 29, pp. 215-219, 2001.

[30] K. Vinoy, "Fractal shaped antenna elements for wide-and multi-band wireless applications," The Pennsylvania State University, 2002.

[31] K. Vinoy, K. Jose, and V. Varadan, "Multi-band characteristics and fractal dimension of dipole antennas with Koch curve geometry," in *Antennas and Propagation Society International Symposium, 2002. IEEE*, 2002, pp. 106-109.

[32] S. Kim, C. Brendle, H.-Y. Lee, M. Walter, S. Gloeggler, S. Krueger, *et al.*, "Evaluation of a 433 MHz band body sensor network for biomedical applications," *Sensors,* vol. 13, pp. 898-917, 2013.